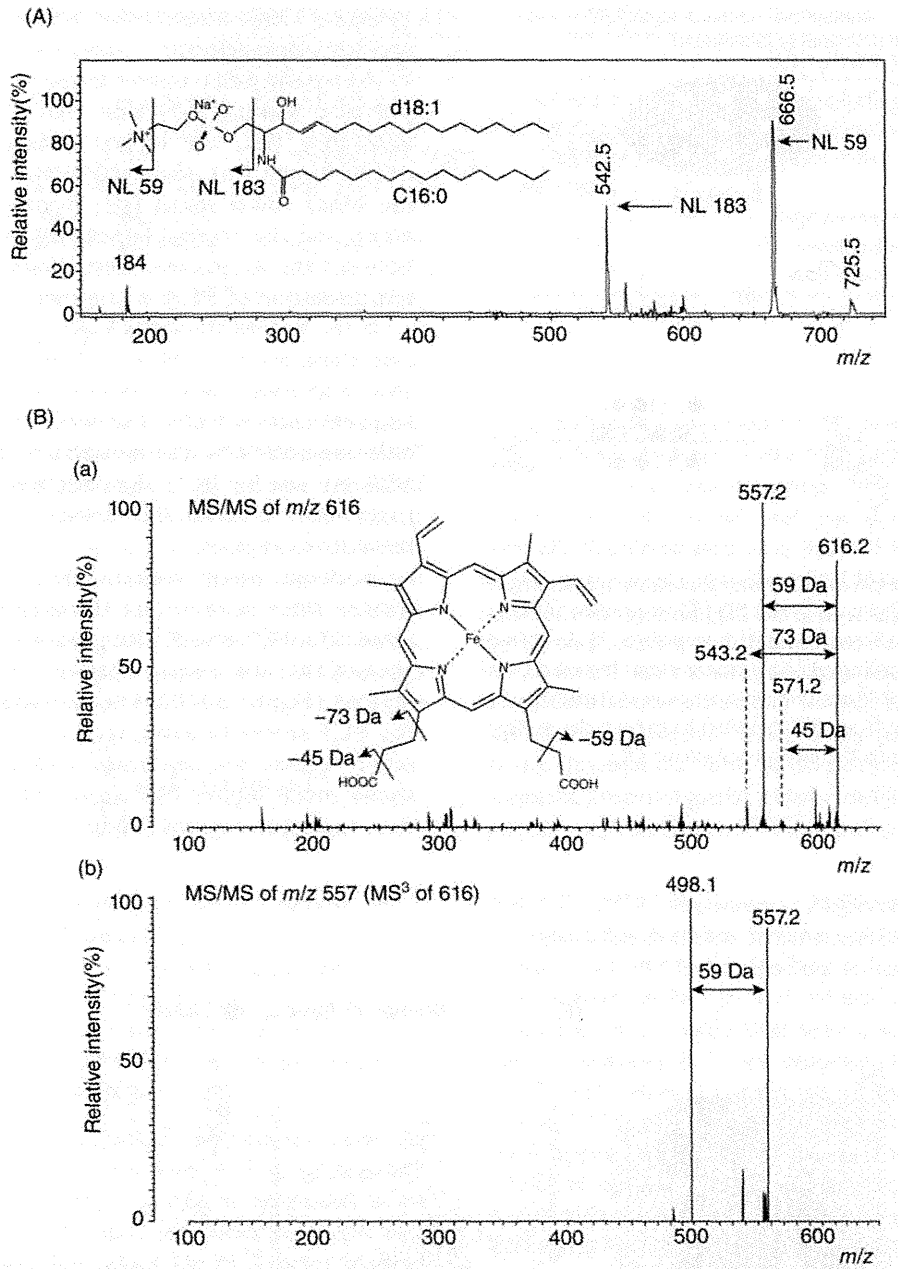

FIGURE 3.39 MS/MS enables the molecular identification of interested ions directly on the tissue surface. A. Product ion mass spectrum on the liver section of *m/z* 725. The NL of 59 and 124 u observed in the spectra is trimethylamine and cyclophosphate, indicating phosphocholine structure. This fragmentation occurred when alkali metal adducted to the precursor ion. The biomolecule of *m/z* 725 was suggested to be the sodiated molecule of SM(16:0). B. Product ion mass spectra on the liver section of *m/z* 616.2 (a) and 557.2 (b). The *m/z* value and fragment patterns indicate that the product ion of *m/z* 616 is heme B. Consecutive NLs of 73, 59, and 45 Da correspond to CH2CH2COOH, CH2COOH, and COOH, respectively. The molecular structure of heme B is shown as an inset in (a).

from a distinct data point on the tissue section. What is important to note is whether two (or several) populations of spectra (= dot) are obtained from distinct regions, for example, normal versus diseased, they are spatially separated on the graph, or not. If they are separated (Figure 3.40A), it means that the molecular expression patterns of these two regions were statistically distinct from each other. If not, PCA failed to extract the statistical differences between the populations (Figure 3.40B).

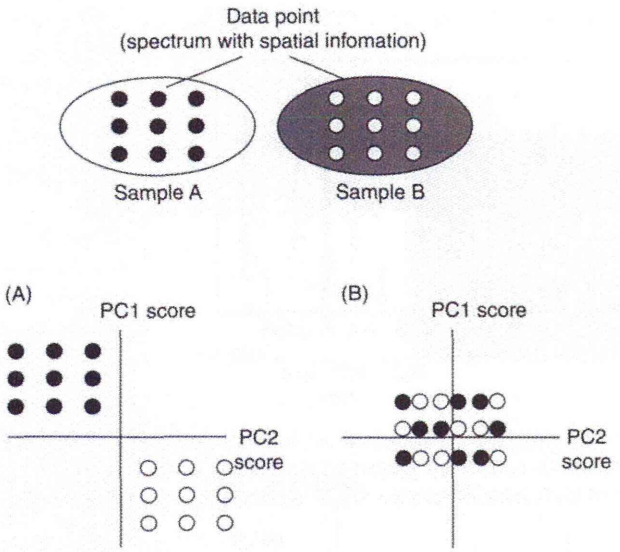

FIGURE 3.40 Example of data interpretation of IMS-linked PCA. In this study, dots seen in the 2D plot represent the *case*, that is, the spectrum from distinct data points. If dots from distinct sample are separated (A), it means that the molecular expression patterns of these two regions were statistically distinct from each other. If not, PCA failed to extract the statistical differences between the two populations (B).

Figure 3.41 shows the result of imaging mass spectrometry–principal component analysis (IMS-PCA) for the colon cancer tissue. In this case, this unsupervised analysis revealed that the largest spectral difference (i.e., the largest difference in metabolite composition) was observed between the normal and the other tissue areas (i.e., normal vs. stroma/cancer area), and the second largest difference was observed between the stroma and normal/cancer area. The overall interpretation of PCA was shown in Table 3.6.

In the graphs shown in Figure 3.41B, the circles indicate mass spectra obtained from the normal, stroma, and cancerous regions (colored white, gray, and black, respectively). Notably, the three populations are spatially separated by the component scores for PC2 and PC3, but not for PC1. This indicates that PC2 and PC3 particularly contain the statistical differences among these three regions.

In detail, along with the PC2 scores (x-axis), the spectra from normal and the others are clearly separated. The PC2 image also demonstrates a large difference of PC2 score value between normal and the other regions (Figure 3.41C). On the other hand, along with the PC3 scores (y-axis), spectra from stroma and the other regions are separated and the PC3 image also shows much higher PC3 score value of stroma region than the other regions (Figure 3.41C).

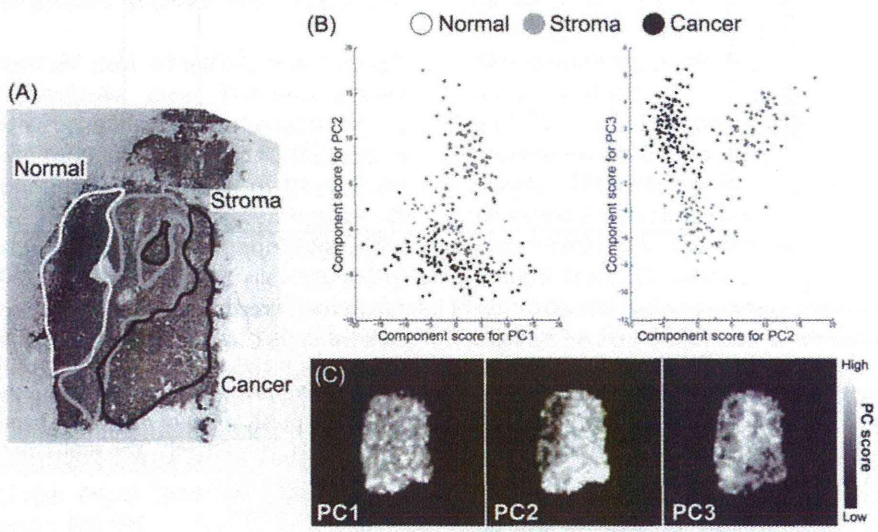

FIGURE 3.41 IMS-linked PCA of colon cancer liver metastasis section revealed altered metabolite compositions among normal stroma and cancer regions. A. Optical images of HE-stained section after IMS measurement representing the normal, stroma, and cancer regions. B. Graphs in which principle component scores for PC1, PC2, and PC3 are plotted. C. Principal component images. According to the value of the principle component score calculated for the spectrum at each tissue location, pixels are indicated with gray value.

TABLE 3.6 The Results and Interpretation of PCA of the Liver Section with Colon Cancer Metastasis

		Primary Contributing PCs			Interpretation of the Component
Component 2	Negative	*m/z* 616.2 (heme B)	*m/z* 828.4 c/t [PC(diacyl-16:0/22:6)+Na]$^+$)	*m/z* 844.4 c/t [PC(diacyl-16:0/22:6)+Na]$^+$)	Representing altered metabolite composition between normal and other regions.
	Positive	*m/z* 744.4	*m/z* 754.4	*m/z* 768.4	
Component 3	Negative	*m/z* 722.0	–	–	Representing altered metabolite composition between stroma and other regions.
	Positive	*m/z* 760.4	*m/z* 766.4		

3.4.3.5 Analysis of Loading Factor for Each Principle Component Facilitates Identification of "Responsible" Molecules Which Differentiate Control and Diseased Samples As a next step, an analysis of the factor loading plot would identify peaks that were differentially expressed between regions. Since a component score defined for each spectrum is a sum of the value of the factor loading value, multiplied by peak intensity, when numbers (= m) of mass peaks were used in the analysis, the component score will be:

$$\text{ScorePC1}(x,y) = \sum_{n=1}^{m} \text{load}(n) \times \text{Int.}(n),$$

where

ScorePC1(x,y) = component score against PC1, obtained from (x, y),
load(n) = factor loading value against a mass peak for n,
Int.(n) = mass peak intensity for n,
m = number of mass peaks used for calculation.

According to this equation, in the spectra from the normal tissue region, the mass peak with large negative value regarding PC2 factor loading is supposed to be intense. On the other hand, it was also indicated that peaks with large positive values for PC2 factor loading would be specific molecules to the stroma/cancerous regions. In other words, such mass peaks with a radical absolute value for PC2 factor loading are suggested to be major contributors to differentiate these regions.

3.4.3.6 PC2 Represents Difference of Metabolite Composition between Normal versus Other Region In Figure 3.42, the factor loading values for PC1 and PC2 are plotted on the x- and y-axes, respectively. Each dot indicates a distinct mass peak. Such a graph makes it very easy to find the peaks with the intended factor loading value against each PC. Since peaks that have negative loading values regarding PC2 are supposed to be specifically expressed by the normal liver cells, we thus picked up mass peaks with large negative loading values for PC2, and obtained their distribution image. As a result, we found that ion at *m/z* 616.2, which is already demonstrated as a normal region-specific molecule, was statistically classified into the *normal region specific* category (Figure 3.42, lower part). Furthermore, by this procedure, other mass peaks corresponding to sodiated and potassiated molecules of PC(diacyl-16:0/22:6) were identified as the normal cell specific metabolites (Figure 3.42, lower part). On the other hand, through the same procedure, we also successfully identified the molecules which localized in the cancerous/stroma region (Figure 3.42, upper part).

3.4.3.7 PC3 Represents Difference of Metabolite Composition between Stroma versus Other Region In Figure 3.43, the factor loading values for PC1 and PC3 are plotted on the x- and y-axes, respectively. In this case, since mass peaks that have a large positive loading value regarding PC3 are supposed to be specific molecules to the stroma region, we picked up the mass peak at *m/z* 722.0 and obtained a distribution image (Figure 3.43, upper part). As a result, we identified ions at *m/z* 722.0 as stroma-specific molecules, and on the other hand, with same procedure, we revealed that ions at *m/z* 760.4 and 766.4 almost disappeared in the stroma region.

3.4.4 Conclusion

Biomarkers are objective indicators of particular pathogenic processes, pharmacological responses, or normal biological states; they can involve any kind of molecule in living organs, for example, proteins, peptides, DNA, and/or metabolites. Biomarkers are essential for the diagnosis and prediction of diseases; IMS can provide distribution information regarding various biomolecules at the cell and tissue levels, and thus it is expected to become a powerful tool for in situ biomarker discovery.

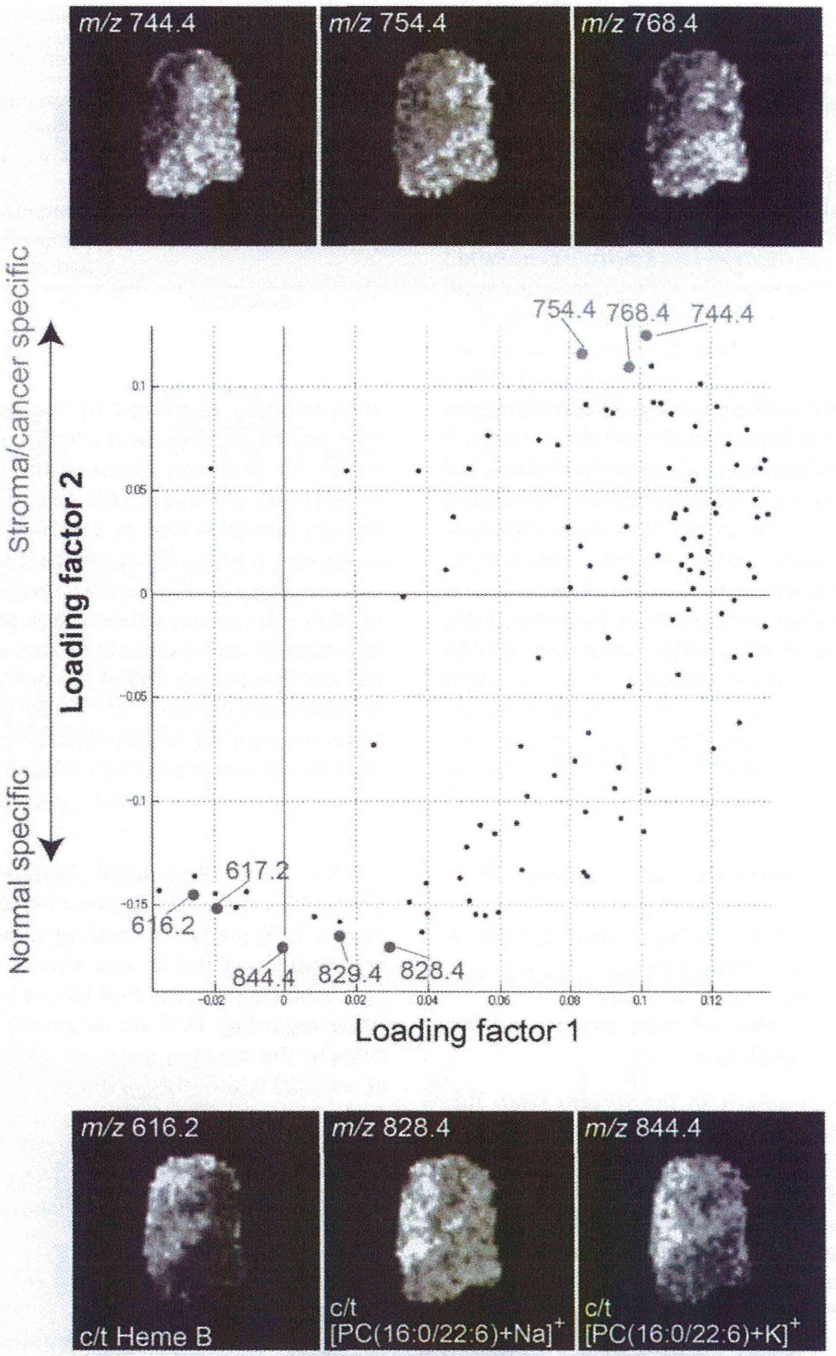

FIGURE 3.42 PC2 represents difference of metabolic composition between normal and other region. In the center graph, factor loading values for PC1 and PC2 are plotted on the *x*- and *y*-axes, respectively. Each dot indicates the distinct mass peak. The peaks with a large positive/negative value for loading factor 2 (i.e., major contributors to differentiation among the groups) were chosen and their distribution images are visualized. c/t, corresponding to.

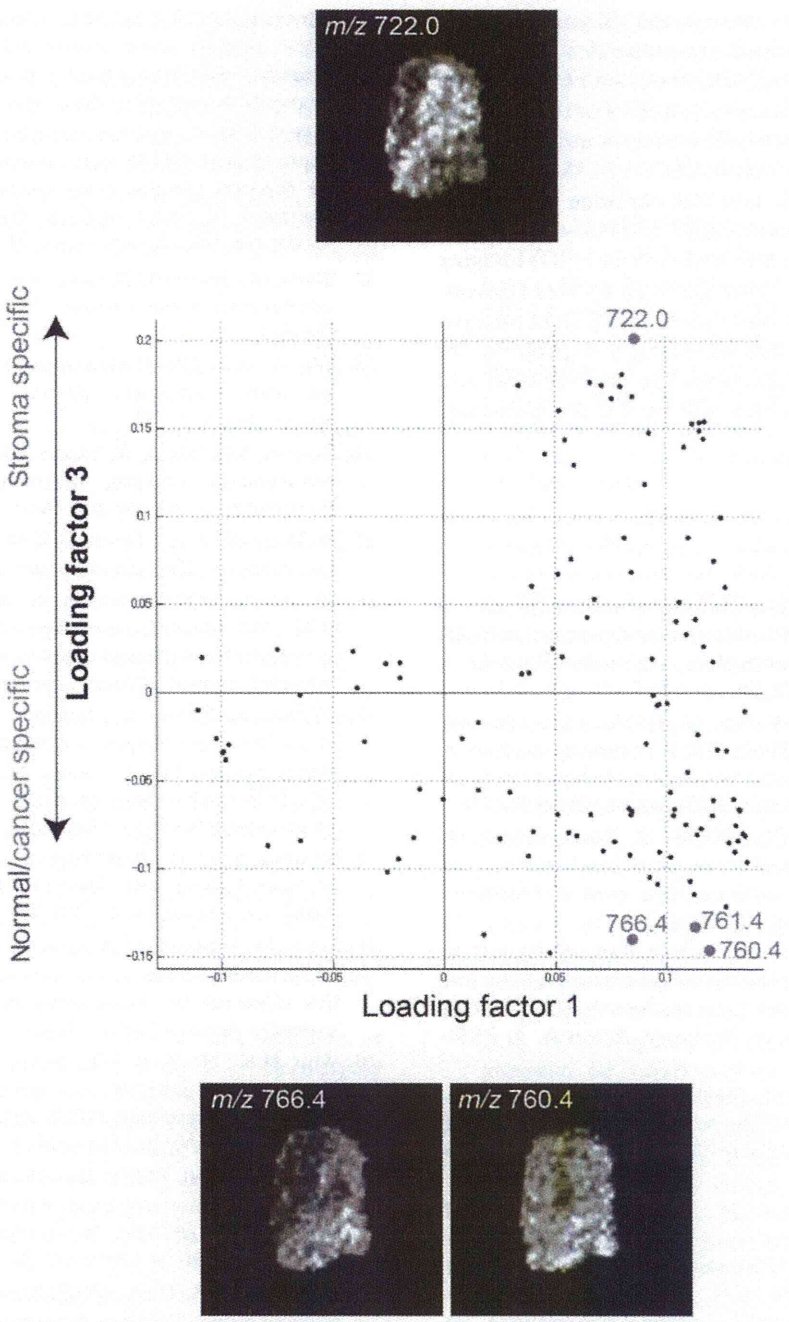

FIGURE 3.43 PC2 represents difference of metabolic composition between normal versus other region. In the center graph, factor loading values for PC1 and PC3 are plotted on the *x*- and *y*-axes, respectively. The mass peaks with large positive/negative value for loading factor 3 were chosen and their distribution images are visualized.

In this chapter, we showed the identification of potential biomarkers, which are molecules that differentiate among the normal, cancerous and even stroma cells in the colon cancer liver metastasis. For this purpose, we showed that the statistical strategy is quite effective to deal with the large volume data set of IMS.

The volumes of IMS data sets continue to increase because of current improvements to IMS with regards to high-resolution [90], three-dimensional (3D) imaging [71], and reconstruction from 3D mass spectra containing ion drift times in ion mobility MS [29]. Data analysis of such large data sets will increasingly depend on the statistical analysis, and therefore the development and application of such analyses will be a more important issue.

REFERENCES

1. Garrett, T.J., et al. (2006) Imaging of small molecules in tissue sections with a new intermediate-pressure MALDI linear ion trap mass spectrometer. *International Journal of Mass Spectrometry*, *260*, 11.
2. Khatib-Shahidi, S., Andersson, M., Herman, J.L., Gillespie, T.A., Caprioli, R.M. (2006) Direct molecular analysis of whole-body animal tissue sections by imaging MALDI mass spectrometry. *Analytical Chemistry*, *78*, 6448–6456.
3. Stoeckli, M., Staab, D., Staufenbiel, M., Wiederhold, K.H., Signor, L. (2002) Molecular imaging of amyloid beta peptides in mouse brain sections using mass spectrometry. *Analytical Biochemistry*, *311*, 33–39.
4. Chaurand, P., Norris, J.L., Cornett, D.S., Mobley, J.A., Caprioli, R.M. (2006) New developments in profiling and imaging of proteins from tissue sections by MALDI mass spectrometry. *Journal of Proteome Research*, *5*, 2889–2900.
5. Krause, E., Wenschuh, H., Jungblut, P.R. (1999) The dominance of arginine-containing peptides in MALDI-derived tryptic mass fingerprints of proteins. *Analytical Chemistry*, *71*, 4160–4165.
6. Gharahdaghi, F., Kirchner, M., Fernandez, J., Mische, S.M. (1996) Peptide-mass profiles of polyvinylidene difluoride-bound proteins by matrix-assisted laser desorption/ionization time-of-flight mass spectrometry in the presence of nonionic detergents. *Analytical Biochemistry*, *233*, 94–99.
7. Annesley, T.M. (2003) Ion suppression in mass spectrometry. *Clinical Chemistry*, *49*, 1041–1044.
8. Jones, J.J., Borgmann, S., Wilkins, C.L., O'Brien, R.M. (2006) Characterizing the phospholipid profiles in mammalian tissues by MALDI FTMS. *Analytical Chemistry*, *78*, 3062–3071.
9. Lemaire, R., et al. (2006) MALDI-MS direct tissue analysis of proteins: Improving signal sensitivity using organic treatments. *Analytical Chemistry*, *78*, 7145–7153.
10. Schwartz, S.A., Reyzer, M.L., Caprioli, R.M. (2003) Direct tissue analysis using matrix-assisted laser desorption/ionization mass spectrometry: practical aspects of sample preparation. *Journal of Mass Spectrometry*, *38*, 699–708.
11. Seeley, E.H., Oppenheimer, S.R., Mi, D., Chaurand, P., Caprioli, R.M. (2008) Enhancement of protein sensitivity for MALDI imaging mass spectrometry after chemical treatment of tissue sections. *Journal of the American Society for Mass Spectrometry*, *19*, 1069–1077.
12. Mann, M., Jensen, O.N. (2003) Proteomic analysis of post-translational modifications. *Nature Biotechnology*, *21*, 255–261.
13. Yan, R., et al. (1999) Membrane-anchored aspartyl protease with Alzheimer's disease beta-secretase activity. *Nature*, *402*, 533–537.
14. Rohner, T.C., Staab, D., Stoeckli, M. (2005) MALDI mass spectrometric imaging of biological tissue sections. *Mechanisms of Ageing and Development*, *126*, 177–185.
15. McDonnell, L.A., Heeren, R.M. (2007) Imaging mass spectrometry. *Mass Spectrometry Reviews*, *26*, 606–643.
16. Groseclose, M.R., Andersson, M., Hardesty, W.M., Caprioli, R.M. (2007) Identification of proteins directly from tissue: in situ tryptic digestions coupled with imaging mass spectrometry. *Journal of Mass Spectrometry*, *42*, 254–262.
17. Shimma, S., Furuta, M., Ichimura, K., Yoshida, Y., Setou, M. (2006) A novel approach to in situ proteome analysis using chemical inkjet printing technology and MALDI-QIT-TOF tandem mass spectrometer. *Journal of the Mass Spectrometry Society of Japan*, *54*, 133–140.
18. Shimma, S., et al. (2008) Mass imaging and identification of biomolecules with MALDI-QIT-TOF-based system. *Analytical Chemistry*, *80*, 878–885.
19. Setou, M., Hayasaka, T., Shimma, S., Sugiura, Y., Matsumoto, M. (2008) Protein denaturation improves enzymatic digestion efficiency for direct tissue analysis using mass spectrometry. *Applied Surface Science*, *255*, 1555–1559.
20. Woo, H.K., Northen, T.R., Yanes, O., Siuzdak, G. (2008) Nanostructure-initiator mass spectrometry: a protocol for preparing and applying NIMS surfaces for high-sensitivity mass analysis. *Nature Protocols*, *3*, 1341–1349.
21. Patti, G.J., et al. (2010) Detection of carbohydrates and steroids by cation-enhanced nanostructure-initiator mass spectrometry (NIMS) for biofluid analysis and tissue imaging. *Analytical Chemistry*, *82*, 121–128.
22. Liu, Q., Guo, Z., He, L. (2007) Mass spectrometry imaging of small molecules using desorption/ionization on silicon. *Analytical Chemistry*, *79*, 3535–3541.
23. Taira, S., et al. (2008) Nanoparticle-assisted laser desorption/ionization based mass imaging with cellular resolution. *Analytical Chemistry*, *80*, 4761–4766.
24. Harada, T., et al. (2009) Visualization of volatile substances in different organelles with an atmospheric-pressure mass microscope. *Analytical Chemistry*, *81*, 9153–9157.
25. Holscher, D., et al. (2009) Matrix-free UV-laser desorption/ionization (LDI) mass spectrometric imaging at the single-cell level: distribution of secondary metabolites of

Arabidopsis thaliana and Hypericum species. *The Plant Journal*, *60*, 907–918.

26. Jackson, S.N., Wang, H.Y., Woods, A.S. (2005) In situ structural characterization of phosphatidylcholines in brain tissue using MALDI-MS/MS. *Journal of the American Society for Mass Spectrometry*, *16*, 2052–2056.
27. Jackson, S.N., Wang, H.Y., Woods, A.S. (2007) In situ structural characterization of glycerophospholipids and sulfatides in brain tissue using MALDI-MS/MS. *Journal of the American Society for Mass Spectrometry*, *18*, 17–26.
28. Rujoi, M., Estrada, R., Yappert, M.C. (2004) In situ MALDI-TOF MS regional analysis of neutral phospholipids in lens tissue. *Analytical Chemistry*, *76*, 1657–1663.
29. McLean, J.A., Ridenour, W.B., Caprioli, R.M. (2007) Profiling and imaging of tissues by imaging ion mobility-mass spectrometry. *Journal of Mass Spectrometry*, *42*, 1099–1105.
30. Sugiura, Y., Setou, M. (2009) Imaging mass spectrometry for visualization of drug and endogenous metabolite distribution: toward in situ pharmacometabolomes. *Journal of Neuroimmune Pharmacology*, *5*, 31–43.
31. Wang, H.Y., Jackson, S.N., Woods, A.S. (2007) Direct MALDI-MS analysis of cardiolipin from rat organs sections. *Journal of the American Society for Mass Spectrometry*, *18*, 567–577.
32. Sugiura, Y., Setou, M. (2009) Selective imaging of positively charged polar and nonpolar lipids by optimizing matrix solution composition. *Rapid Communications in Mass Spectrometry*, *23*, 3269–3278.
33. Han, X., Gross, R.W. (2001) Quantitative analysis and molecular species fingerprinting of triacylglyceride molecular species directly from lipid extracts of biological samples by electrospray ionization tandem mass spectrometry. *Analytical Biochemistry*, *295*, 88–100.
34. Hsu, F.F., Turk, J. (2001) Structural determination of glycosphingolipids as lithiated adducts by electrospray ionization mass spectrometry using low-energy collisional-activated dissociation on a triple stage quadrupole instrument. *Journal of the American Society for Mass Spectrometry*, *12*, 61–79.
35. Piomelli, D., Astarita, G., Rapaka, R. (2007) A neuroscientist's guide to lipidomics. *Nature Reviews. Neuroscience*, *8*, 743–754.
36. Hitzemann, R.J., Johnson, D.A. (1983) Developmental changes in synaptic membrane lipid composition and fluidity. *Neurochemical Research*, *8*, 121–131.
37. Zerouga, M., Jenski, L.J., Stillwell, W. (1995) Comparison of phosphatidylcholines containing one or two docosahexaenoic acyl chains on properties of phospholipid monolayers and bilayers. *Biochimica et Biophysica Acta*, *1236*, 266–272.
38. Ostrowski, S.G., Van Bell, C.T., Winograd, N., Ewing, A.G. (2004) Mass spectrometric imaging of highly curved membranes during Tetrahymena mating. *Science*, *305*, 71–73.
39. Murakami, M., Nakatani, Y., Atsumi, G., Inoue, K., Kudo, I. (1997) Regulatory functions of phospholipase A2. *Critical Reviews in Immunology*, *17*, 225–283.
40. Astarita, G., Ahmed, F., Piomelli, D. (2008) Identification of biosynthetic precursors for the endocannabinoid anandamide in the rat brain. *Journal of Lipid Research*, *49*, 48–57.
41. Sugiura, Y., et al. (2009) Visualization of the cell-selective distribution of PUFA-containing phosphatidylcholines in mouse brain by imaging mass spectrometry. *Journal of Lipid Research*, *50*, 1776–1788.
42. Salem, N., Jr., Litman, B., Kim, H.Y., Gawrisch, K. (2001) Mechanisms of action of docosahexaenoic acid in the nervous system. *Lipids*, *36*, 945–959.
43. Kim, H.Y. (2007) Novel metabolism of docosahexaenoic acid in neural cells. *The Journal of Biological Chemistry*, *282*, 18661–18665.
44. Stubbs, C.D., Smith, A.D. (1984) The modification of mammalian membrane polyunsaturated fatty acid composition in relation to membrane fluidity and function. *Biochimica et Biophysica Acta*, *779*, 89–137.
45. van Echten, G., Sandhoff, K. (1993) Ganglioside metabolism. Enzymology, topology, and regulation. *The Journal of Biological Chemistry*, *268*, 5341–5344.
46. Sonnino, S., Chigorno, V. (2000) Ganglioside molecular species containing C18- and C20-sphingosine in mammalian nervous tissues and neuronal cell cultures. *Biochimica et Biophysica Acta*, *1469*, 63–77.
47. Sambasivarao, K., McCluer, R.H. (1964) Lipid components of gangliosides. *Journal of Lipid Research*, *15*, 103–108.
48. Schwarz, H.P., Kostyk, I., Marmolejo, A., Sarappa, C. (1967) Long-chain bases of brain and spinal cord of rabbits. *Journal of Neurochemistry*, *14*, 91–97.
49. Jungalwala, F.B., Hayssen, V., Pasquini, J.M., McCluer, R.H. (1979) Separation of molecular species of sphingomyelin by reversed-phase high-performance liquid chromatography. *Journal of Lipid Research*, *20*, 579–587.
50. Palestini, P., Sonnino, S., Tettamanti, G. (1991) Lack of the ganglioside molecular species containing the C20-long-chain bases in human, rat, mouse, rabbit, cat, dog, and chicken brains during prenatal life. *Journal of Neurochemistry*, *56*, 2048–2050.
51. Palestini, P., Masserini, M., Sonnino, S., Giuliani, A., Tettamanti, G. (1990) Changes in the ceramide composition of rat forebrain gangliosides with age. *Journal of Neurochemistry*, *54*, 230–235.
52. Mansson, J.E., Vanier, M.T., Svennerholm, L. (1978) Changes in the fatty acid and sphingosine composition of the major gangliosides of human brain with age. *Journal of Neurochemistry*, *30*, 273–275.
53. Kotani, M., Kawashima, I., Ozawa, H., Terashima, T., Tai, T. (1993) Differential distribution of major gangliosides in rat central nervous system detected by specific monoclonal antibodies. *Glycobiology*, *3*, 137–146.

54. Jackson, S.N., Wang, H.Y., Woods, A.S. (2005) Direct profiling of lipid distribution in brain tissue using MALDI-TOFMS. *Analytical Chemistry*, *77*, 4523–4527.

55. Hayasaka, T., et al. (2008) Matrix-assisted laser desorption/ionization quadrupole ion trap time-of-flight (MALDI-QIT-TOF)-based imaging mass spectrometry reveals a layered distribution of phospholipid molecular species in the mouse retina. *Rapid Communications in Mass Spectrometry*, *22*, 3415–3426.

56. Chen, Y., et al. (2008) Imaging MALDI mass spectrometry using an oscillating capillary nebulizer matrix coating system and its application to analysis of lipids in brain from a mouse model of Tay-Sachs/Sandhoff disease. *Analytical Chemistry*, *80*, 2780–2788.

57. Cornett, D.S., Frappier, S.L., Caprioli, R.M. (2008) MALDI-FTICR imaging mass spectrometry of drugs and metabolites in tissue. *Analytical Chemistry*, *80*, 5648–5653.

58. Jackson, S.N., et al. (2007) MALDI-ion mobility-TOFMS imaging of lipids in rat brain tissue. *Journal of Mass Spectrometry*, *42*, 1093–1098.

59. Amantonico, A., Oh, J.Y., Sobek, J., Heinemann, M., Zenobi, R. (2008) Mass spectrometric method for analyzing metabolites in yeast with single cell sensitivity. *Angewandte Chemie International Edition,*, *47*, 5382–5385.

60. Burrell, M., Earnshaw, C., Clench, M. (2007) Imaging matrix assisted laser desorption ionization mass spectrometry: a technique to map plant metabolites within tissues at high spatial resolution. *Journal of Experimental Botany*, *58*, 757–763.

61. Benabdellah, F., Touboul, D., Brunelle, A., Laprevote, O. (2009) In situ primary metabolites localization on a rat brain section by chemical mass spectrometry imaging. *Analytical Chemistry*, *81*, 5557–5560.

62. Knowles, J.R. (1980) Enzyme-catalyzed phosphoryl transfer reactions. *Annual Review of Biochemistry*, *49*, 877–919.

63. Stoeckli, M., Staab, D., Schweitzer, A. (2006) Compound and metabolite distribution measured by MALDI mass spectrometric imaging in whole-body tissue sections. *International Journal of Mass Spectrometry*, *260*, 195–202.

64. Umemura, A., Mabe, H., Nagai, H., Sugino, F. (1992) Action of phospholipases A2 and C on free fatty acid release during complete ischemia in rat neocortex. Effect of phospholipase C inhibitor and N-methyl-D-aspartate antagonist. *Journal of Neurosurgery*, *76*, 648–651.

65. Rehncrona, S., Westerberg, E., Akesson, B., Siesjo, B.K. (1982) Brain cortical fatty acids and phospholipids during and following complete and severe incomplete ischemia. *Journal of Neurochemistry*, *38*, 84–93.

66. Sugiura, Y., Shimma, S., Setou, M. (2006) Thin sectioning improves the peak intensity and signal-to-noise ratio in direct tissue mass spectrometry. *Journal of the Mass Spectrometry Society of Japan*, *54*, 4.

67. Scherl, A., et al. (2005) Gold coating of non-conductive membranes before matrix-assisted laser desorption/ionization tandem mass spectrometric analysis prevents charging effect. *Rapid Communications in Mass Spectrometry*, *19*, 605–610.

68. Chaurand, P., Schwartz, S.A., Caprioli, R.M. (2002) Imaging mass spectrometry: a new tool to investigate the spatial organization of peptides and proteins in mammalian tissue sections. *Current Opinion in Chemical Biology*, *6*, 676–681.

69. Stoeckli, M., Chaurand, P., Hallahan, D.E., Caprioli, R.M. (2001) Imaging mass spectrometry: a new technology for the analysis of protein expression in mammalian tissues. *Nature Medicine*, *7*, 493–496.

70. Goodwin, R.J., Pennington, S.R., Pitt, A.R. (2008) Protein and peptides in pictures: imaging with MALDI mass spectrometry. *Proteomics*, *8*, 3785–3800.

71. Andersson, M., Groseclose, M.R., Deutch, A.Y., Caprioli, R.M. (2008) Imaging mass spectrometry of proteins and peptides: 3D volume reconstruction. *Nature Methods*, *5*, 101–108.

72. Altelaar, A.F., et al. (2006) Gold-enhanced biomolecular surface imaging of cells and tissue by SIMS and MALDI mass spectrometry. *Analytical Chemistry*, *78*, 734–742.

73. Goodwin, R.J., Dungworth, J.C., Cobb, S.R., Pitt, A.R. (2008) Time-dependent evolution of tissue markers by MALDI-MS imaging. *Proteomics*, *8*, 3801–3808.

74. Murphy, R.C., LIPID MAPS Lipidomics Workshop. (2009) Future directions: tissue and cell imaging. Available at http://www.lipidmaps.org/resources/lipidmapspresentations/EB2009/MurphyEB2009.pdf.

75. Sugiura, Y., Shimma, S., Setou, M. (2006) Two-step matrix application technique to improve ionization efficiency for matrix-assisted laser desorption/ionization in imaging mass spectrometry. *Analytical Chemistry*, *78*, 8227–8235.

76. Mock, K.K., Sutton, C.W., Cottrell, J.S. (1992) Sample immobilization protocols for matrix-assisted laser-desorption mass spectrometry. *Rapid Communications in Mass Spectrometry*, *6*, 233–238.

77. Yanagisawa, K., et al. (2003) Proteomic patterns of tumour subsets in non-small-cell lung cancer. *Lancet*, *362*, 433–439.

78. Ajiki, W., Tsukuma, H., Oshima, A. (2004) Survival rates of childhood cancer patients in Osaka, Japan. *Japanese Journal of Clinical Oncology*, *34*, 50–54.

79. Harkins, L., et al. (2002) Specific localisation of human cytomegalovirus nucleic acids and proteins in human colorectal cancer. *Lancet*, *360*, 1557–1563. Elsevier.

80. Newell, G.R., Spitz, M.R., Sider, J.G. (1989) Cancer and age. *Seminars in Oncology*, *16*, 3–9.

81. Kuriki, K., et al. (2006) Risk of colorectal cancer is linked to erythrocyte compositions of fatty acids as biomarkers for dietary intakes of fish, fat, and fatty acids. *Cancer Epidemiology, Biomarkers & Prevention*, *15*, 1791–1798.

82. Huerta, S., et al. (2003) Gene expression profile of metastatic colon cancer cells resistant to cisplatin-induced apoptosis. *International Journal of Oncology* *22*, 663–670.

83. Demirev, P.A., et al. (2002) Detection of malaria parasites in blood by laser desorption mass spectrometry. *Analytical Chemistry*, *74*, 3262–3266.

84. Rael, L.T., Ayala-Fierro, F., Bar-Or, R., Carter, D.E., Barber, D.S. (2006) Interaction of arsine with hemoglobin in arsine-induced hemolysis. *Toxicological Sciences*, *90*, 142–148.

85. Dueck, D.A., et al. (1996) The modulation of choline phosphoglyceride metabolism in human colon cancer. *Molecular and Cellular Biochemistry*, *162*, 97–103.

86. Dobrzyńska, I., Szachowicz-Petelska, B., Sulkowski, S., Figaszewski, Z. (2005) Changes in electric charge and phospholipids composition in human colorectal cancer cells. *Molecular and Cellular Biochemistry*, *276*, 113–119.

87. Brasitus, T.A., Dudeja, P.K., Dahiya, R. (1986) Premalignant alterations in the lipid composition and fluidity of colonic brush border membranes of rats administered 1, 2 dimethylhydrazine. *Journal of Clinical Investigation*, *77*, 831–840.

88. Stark, D.D., Wittenberg, J., Butch, R.J., Ferrucci, J.T. (1987) Hepatic metastases: randomized, controlled comparison of detection with MR imaging and CT. *Radiology*, *165*, 399–406.

89. Stark, D.D., et al. (1988) Superparamagnetic iron oxide: clinical application as a contrast agent for MR imaging of the liver. *Radiology*, *168*, 297–301.

90. McDonnell, L.A., et al. (2005) Subcellular imaging mass spectrometry of brain tissue. *Journal of Mass Spectrometry*, *40*, 160–168.

91. Chaurand, P., et al. (2004) Integrating histology and imaging mass spectrometry. *Analytical Chemistry*, *76*, 1145–1155.

92. Astigarraga, E., Barreda-Gómez, G., Lombardero, L., Fresnedo, O., Castaño, F., et al. (2008) Profiling and imaging of lipids on brain and liver tissue by matrix-assisted laser desorption/ionization mass spectrometry using 2-mercaptobenzothiazole as a matrix. *Analytical Chemistry*, *80*, 9105–9114.

93. Sugiura, Y., Shimma, S., Konishi, Y., Yamada, M.K., Setou, M. (2008) Imaging mass spectrometry technology and application on ganglioside study; visualization of age-dependent accumulation of C20-ganglioside molecular species in the mouse hippocampus. *PLoS ONE*, *3*, e3232.

94. Ageta, H., Asai, S., Sugiura, Y., Goto-Inoue, N., Zaima, N., Setou, M. (2009) Layer-specific sulfatide localization in rat hippocampus middle molecular layer is revealed by nanoparticle-assisted laser desorption/ionization imaging mass spectrometry. *Medical Molecular Morphology*, *42*, 16–23.

95. Cha, S., Yeung, E.S. (2007) Colloidal graphite-assisted laser desorption/ionization mass spectrometry and MSn of small molecules. 1. Imaging of cerebrosides directly from rat brain tissue. *Analytical Chemistry*, *79*, 2373–2385.

96. Zhang, H., Cha, S., Yeung, E.S., (2007) Colloidal graphite-assisted laser desorption/ionization MS and MS(n) of small molecules. 2. Direct profiling and MS imaging of small metabolites from fruits. *Analytical Chemistry*, *79*, 6575–6584.

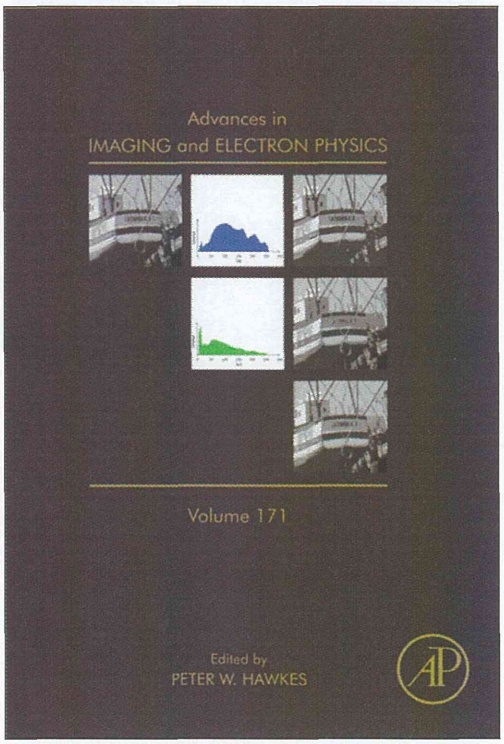

From Kamlesh Shrivas and Mitsutoshi Setou, Imaging Mass Spectrometry:
Sample Preparation, Instrumentation, and Applications.
In: Peter W. Hawkes, editor, Advances in Imaging and Electron Physics, Vol 171.
San Diego: Academic Press, 2012, pp. 145–193.
ISBN: 978-0-12-394297-5